

Two-dimensional oscillatory patterns in semiconductors with point contacts

L. L. Bonilla and R. Escobedo

Escuela Politécnica Superior, Universidad Carlos III de Madrid, 28911 Leganés, Spain

(Received 17 January 2001; published 14 August 2001)

Planar samples of n -GaAs with attached point contacts at different dc voltages may display a variety of spatiotemporal patterns arising from the dynamics of curved charge dipole waves. Patterns rank from oscillations due to recycling and motion of simple quasiplanar or cylindrical wave fronts to more complex patterns that include merging and splitting of different fronts. Results of numerical simulations are interpreted by means of simple one-dimensional asymptotic theories.

DOI: 10.1103/PhysRevE.64.036203

PACS number(s): 05.45.-a, 85.30.Fg, 47.54.+r

Self-sustained oscillations of the electric current in dc voltage biased semiconductors presenting a N -shaped local current-field characteristics are typically due to recycling and motion of charge density waves [1–4]. Typical cases are the Gunn effect in bulk n -GaAs [5,6], slow current oscillations in materials where trap dynamics is important such as ultra-pure p -Ge [7] and semi-insulating GaAs [8,9], and superlattices [10,11], etc. These self-oscillations may be time periodic, quasiperiodic or chaotic [4,7,10–14]. So far, most of the studies deal with quasi-one-dimensional geometries, for which the physical and mathematical mechanisms resulting in self-oscillations are reasonably well understood [1,2,15,16]. The situation is quite different in two or three space dimensions, where experimental data [8] or theoretical studies are scarce. Two-dimensional geometries can be easily achieved by attaching point contacts to planar samples, made out of either bulk materials or of heterostructures in horizontal transport.

In this paper, we numerically simulate a well-known model of the Gunn effect (due to Kroemer [6]) on a planar sample with point contacts at different voltages. We find a variety of spatiotemporal patterns generated by recycling, motion and interaction of charge dipole waves, which emanate from different contacts. Patterns rank from simple quasi one-dimensional pattern (either one-dimensional Gunn effect or cylindrically symmetric Gunn effect) to more complex patterns.

Kroemer's model consists of the Poisson and charge continuity equations for the concentration of free carriers (electrons) $n(\vec{x}, t)$ and the electric potential $\varphi(\vec{x}, t)$:

$$\epsilon \vec{\nabla}^2 \varphi = e(n - N_D), \quad (1)$$

$$\frac{\partial n}{\partial t} + \vec{\nabla} \cdot (n\vec{v} - D \vec{\nabla} n) = 0. \quad (2)$$

Here \vec{v} is the carrier drift velocity that is a function of the electric field as depicted in Fig. 1. For numerical calculations, we shall use the specific form, $\vec{v} = \mu_0 E_R \vec{v}(E/E_R)$, where $\vec{v}(E) = \vec{E} (1 + v_s E^3)/(1 + E^4)$, with $E = |\vec{E}|$, and $E_R \approx 4$ kV/cm. At high fields, the velocity reaches a saturation value, $\mu_0 E_R v_s$. μ_0 , $D = \mu_0 k_B T/e$, ϵ , $N_D \approx 10^{15}$ cm $^{-3}$, and e are zero field mobility, diffusion coefficient (assumed to be constant for simplicity), permittivity, doping, and the charge

of the electron, respectively. $\vec{E} = -\vec{\nabla} \varphi$ is minus the electric field. We shall write these equations in nondimensional form by adopting E_R , N_D , $l_1 = \epsilon E_R / (e N_D) \approx 0.276$ μ m, $l_1 / (\mu_0 E_R) \approx 1.02$ ps, and $E_R l_1 \approx 0.011$ V, as the units of field, electron density, length, time, and potential, respectively. In these units, we can set all coefficients in the previous equations equal to one, except for writing a dimensionless diffusion coefficient, $\delta \approx 0.013$ (at 20 K).

The function $\vec{v}(E)$ is already written in dimensionless units. We can write an Ampère's equation for the total current density, \vec{J} , by eliminating n from Eq. (2) using Eq. (1). In nondimensional form, the result is

$$\frac{\partial \vec{E}}{\partial t} + \vec{v}(1 + \vec{\nabla} \cdot \vec{E}) - \delta \vec{\nabla}[\vec{\nabla} \cdot \vec{E}] = \vec{J}, \quad (3)$$

with $\vec{\nabla} \cdot \vec{J} = 0$.

Boundary conditions are chosen as follows. At the interfaces between semiconductor and contacts, $\Sigma_{c,a}$, we assume the normal components of electron current density and electric field are proportional (Ohm's law) [2,15], $\vec{E} \cdot \vec{N} = \rho(n\vec{v} - \delta \vec{\nabla} n) \cdot \vec{N}$ (N is the unit normal to $\Sigma_{c,a}$, directed towards the semiconductor). For simplicity, we choose all contact resistivities ρ to be equal. Bias conditions are chosen to be φ

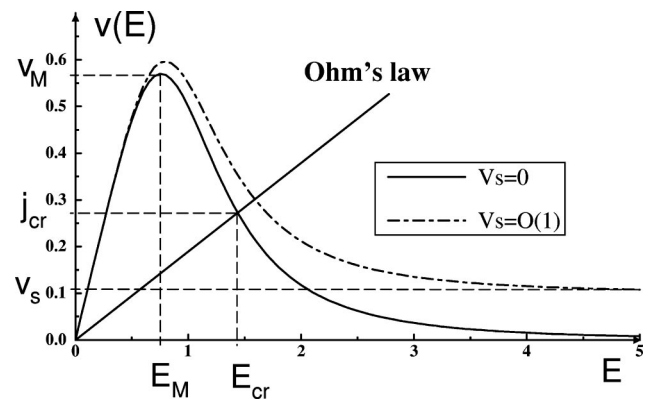


FIG. 1. Dimensionless drift velocity curve as a function of electric field for two different saturation values v_s . Contact resistivity is chosen so that the boundary current density $j = E/\rho$ intersects $v(E)$ on its second branch, past the maximum (E_M, v_M) , as shown in the figure.

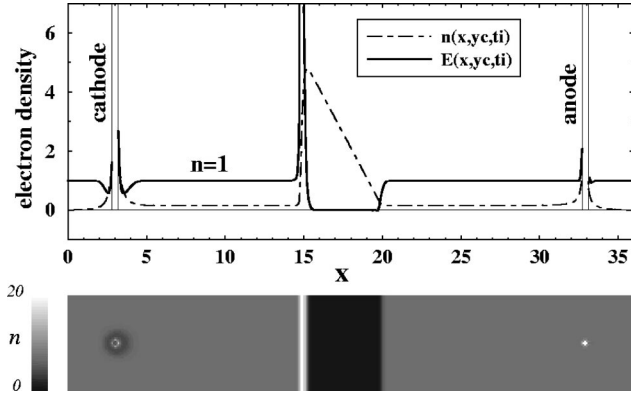


FIG. 2. Upper part: spatial profiles of electron density (solid line) and electric field (dot-dash line) at $y = y_c$ and $t = t_i$, exactly corresponding to the density plot of $n(x, y_c, t_i)$ in the 36×6 rectangular sample in the lower part of the figure. Outside the dipole wave and contact regions (cathode on the left, anode on the right, separated a distance $L = 30$) $n = 1$.

$= 0$ at cathodes Σ_c (injecting contacts) and $\varphi = \phi$ at anodes Σ_a (receiving contacts). At the physical boundary of the sample there are no contacts, and we adopt homogeneous Neumann conditions there, $\vec{\nabla} \varphi \cdot \vec{N} = 0 = \vec{\nabla} n \cdot \vec{N}$. With these conditions, our choice of sample and point contacts, and an initial profile for n at $t = 0$, we can start numerical simulations of the multidimensional Kroemer's model. Numerical simulations show the time evolution of current through a receiving contact, $i(t) = \int_{\Sigma_a} \vec{J} \cdot \vec{N} dA$, and of the electron density profile, $n(x, y, t)$. The latter is depicted in a gray scale that goes from black for $n = 0$ to white for the maximum positive value of n ; see Fig. 2. The simplest situation is obtained when only one cathode and one anode are situated far from each other, near the ends of a rectangular sample, as in Fig. 2 ($L_x = 36$, $L_y = 6$, contact separation is $L = 30$). For appropriate bias, the electric current shows self-oscillations consisting of a periodic array of spikes separated by regions where the current is flat; see Fig. 3. These current traces are typical of the one-dimensional (1D) case [15]. The charge distribution in Fig. 2 corresponds to times selected on the flat portion of the time traces of the current $i(t)$ in Fig. 3. Evolution of the electron density corresponds to repeated nucle-

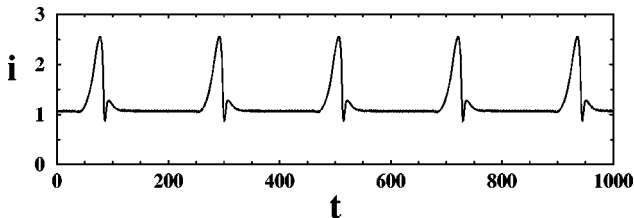


FIG. 3. Self-oscillations of the current on the rectangular sample of Fig. 2 for bias $\phi = 18$. Oscillation period is $T = 215$, $i(t)$ is approximately 1.07 during a time $T_{trip} = 135$, corresponding to the trip of a planar dipole wave from cathode to anode. The current spike (lasting $T_{relief} = 80$) appears during wave creation and annihilation at contacts. Extrema of $i(t)$ are $i_{max} = 2.56$ and $i_{min} = 0.87$. In this and successive figures, the scale of $i(t)$ has been divided by 50.

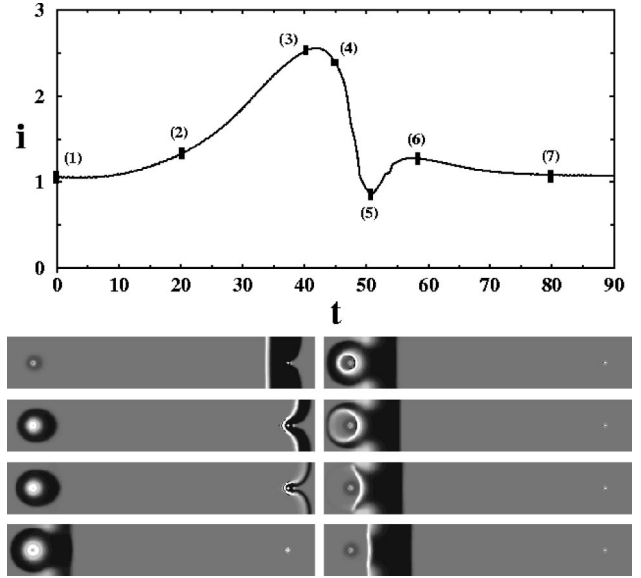


FIG. 4. Details of wave annihilation and creation processes when the current trace of Fig. 3 presents a spike (upper part of figure). Lower part, from left to right and top to bottom: electron density profiles at the times marked on the current trace. After the last situation depicted, the current is almost constant, the dipole front is planar, and it moves undisturbed until it reaches the anode.

ation of a dipole wave at the cathode, undisturbed motion as a flat front towards the anode and annihilation there; see Figs. 2–4.

A more precise analysis of our data shows that the motion of the flat dipole far from the contacts is 1D. In terms of the electric field, the wave is an isosceles triangle of base and height $E_+ \approx \sqrt{2\phi} = 6$ if $\phi = 18$, according to the asymptotic theory of Ref. [15], which neglects the field outside the dipole wave. Simulation data gives $E_+ \approx 5$. The wave velocity is $V \approx \pi/(4E_+) = \pi/20 \approx 0.157$. The wave moves undisturbed a distance $L_{trip} \approx 22$ (contact separation is 30, minus the size of the wave after nucleation, $s_n = 3$, minus the size of the fully formed wave as it arrives at the anode, $s_a = 5$). To traverse this distance, the wave should therefore spend a time $T_{trip} = L_{trip}/V \approx 140$, which is very similar to that in numerical simulations, i.e. 135; see Fig. 3. During its creation, the dipole wave is almost circular. This particular stage could, therefore, be described by a sample with Corbino symmetry: a circular sample surrounded by a circular anode and enclosing a point cathode at its center [17].

It is not necessary to use a Corbino geometry to observe an axisymmetric Gunn effect. We can achieve this symmetry placing a cathode (with $\phi = 0$) at the center of a square with four anodes symmetrically located near its vertices; see Fig. 5. Notice that the wave is annihilated before it can reach the anodes: both the wave width and height decrease until it disappears.

To understand the axisymmetric case, we can write Eq. (3) in polar coordinates and integrate its radial component with respect to the polar angle. The result is

$$\frac{\partial E}{\partial t} + v(E) \left[1 + \frac{1}{r} \frac{\partial(rE)}{\partial r} \right] - \delta \frac{\partial}{\partial r} \left[\frac{1}{r} \frac{\partial(rE)}{\partial r} \right] = \frac{J}{r}. \quad (4)$$

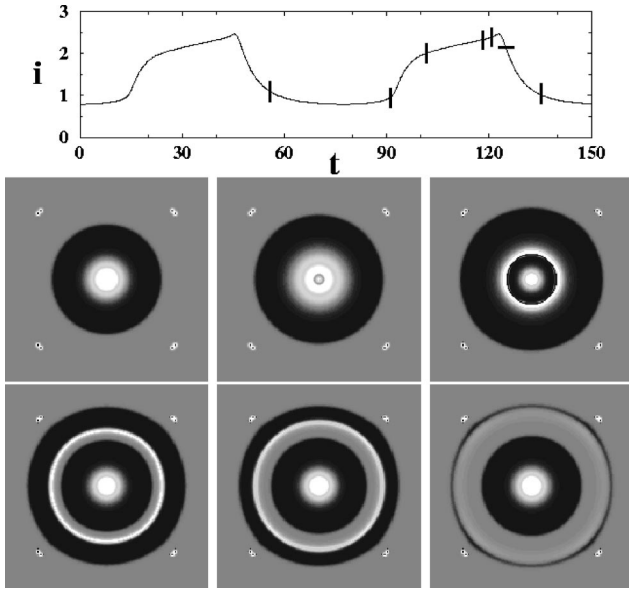


FIG. 5. Upper part: current traces for the axisymmetric case. The sample is a square of side $L=18$, with a central cathode ($\phi=0$) and four identical anodes ($\phi=18$) at $d=3$ from its boundary. Distance between cathode and one anode is $L=15/\sqrt{2}\approx 10.6$. Oscillation period, maximum, and minimum values of the current are $T=77.5$, $i_{max}=2.47$, and $i_{min}=0.79$, respectively. Lower part of figure, from left to right and top to bottom: Density plots corresponding to the times 0, 36, 50, 64, 66, and 69 marked in the upper part.

Here the total current density is directed along the radial direction, and the function J depends only on time. The bias condition is simply $\int_{r_c}^{r_a} E(r,t) dr = \phi$, where r_c and r_a are the contact radii in a Corbino geometry. In terms of the point contacts located at the origin (center of the square sample) and at $\vec{x}_a^{(k)}$, $k=1,2,3,4$, r_c is the radius of a point contact, while $r_a=|\vec{x}_a^{(k)}|-r_c$. We want to understand the more salient features of the Gunn oscillation in this case: the shape of $i(t)$ and the fact that the dipole wave vanishes before reaching the anode. It is easier to understand the case when $r_a \gg r_c \gg 1$, for dipole waves are detached from the contacts most of the time. To analyze the Gunn effect, we need to study the boundary layers near inner and outer contacts, and to describe a dipole wave far from them. These analysis are fairly technical, so that we will give here few indications only [18]. A dipole wave detached from the contacts is a straight triangle of height $E_+ - E_-$ and base $R_l - R_b$, which are all time-dependent parameters. It is made of a trailing front at $r=R_b(t)$, which is a shock wave (moving at a speed given by the equal area rule), and a leading front at $r=R_l(t)$, which is a region depleted of electrons [15]. We shall see that the trailing front increases its speed as it advances, whereas the speed of the leading front decreases. This explains why the wave vanishes before reaching the anode (which is far from the cathode). The electron density at the leading front is almost zero, so that the field obeys the Poisson equation, $n=1+r^{-1}\partial(rE)/\partial r$, with $n=0$, which yields:

$$E(r,t) = \frac{r_w^2(t) - r^2}{2r}, \quad r \in [R_b(t), R_l(t)]. \quad (5)$$

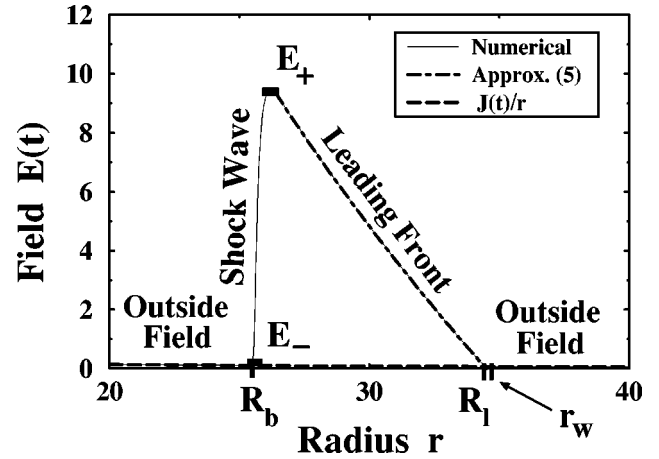


FIG. 6. Electric field profile and asymptotic approximations of the leading front and the outer field. $R_b(t)$, position of shock wave; $R_l(t)$, position of the intersection between leading front and outside field; $E_+(t)$, wave height; $E_-(t)$, outside field at $r=R_b(t)$; field outside wave is $J(t)/r$. At $r=r_w(t)$, the field in the leading front vanishes.

Here the constant of integration $r_w(t)$ is the intersection between the prolongation of the leading front and the r axis. See Fig. 6.

The velocity of the leading front, dr_w/dt , can be obtained by insertion of Eq. (5) and $n=0$ into Eq. (4), which yields

$$\frac{dr_w}{dt} = \frac{J}{r_w}. \quad (6)$$

Then $r_w(t) = \sqrt{2 \int J(t) dt}$ instead of $\int J(t) dt$, as in the 1D case [15]. The velocity of the trailing front, dR_b/dt , is given by the equal area rule for shock waves [15], $dR_b/dt = V(E_+, E_-) \equiv [1/(E_+ - E_-)] \int_{E_-}^{E_+} v(E) dE$. If $v_s=0$, $V(E_+, E_-) = \frac{1}{2} (\arctan E_+^2 - \arctan E_-^2) / (E_+ - E_-)$, which gives

$$\frac{dR_b}{dt} = \frac{\pi}{4E_+}, \quad (7)$$

when $E_+ \gg 1 \gg E_-$ (which occurs in the limit we are considering). Thus the trailing front velocity is small and small waves move faster than large ones.

Typically in our simulations, we have the following relation $r_w \gg (r_w - R_b) \gg 1$. In this limit, the slope of the electric field in the leading front, given by Eq. (5), is -1 , so that $E(r,t) \sim r_w - r$ inside the dipole wave and $R_l - R_b = E_+ - E_- \approx E_+$. Then, as $E[R_b(t), t] = E_+(t)$ in the leading front, we have:

$$E_+(t) = r_w(t) - R_b(t), \quad (8)$$

and furthermore $R_l \approx r_w$. As the dipole moves, E_+ decreases because $dr_w/dt < dR_b/dt$, and the wave vanishes before arriving at the anode. Notice that Eq. (6), (7), and (8) imply that the area inside the dipole, $\phi_{in} \sim E_+^2/2$, decreases as $d\phi_{in}/dt = JE_+/r_w - \pi/4$.

To determine the shape of the current traces, $i(t) = 2\pi J(t)$, we need an additional evolution equation for J .

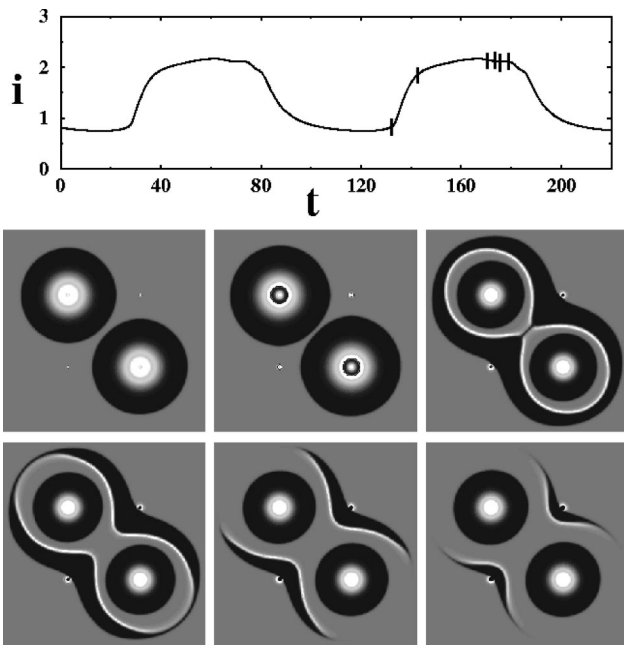


FIG. 7. Same as in Fig. 5 for a configuration with two cathodes ($\phi=0$) and two anodes ($\phi=26$) placed at the vertices of a square. Sample side is $L=28$. Oscillation period, maxima, and minima are $T=105.2$, $i_{max}=2.17$, and $i_{min}=0.74$, respectively. Density plots in the lower part of the figure correspond to the times 0, 11, 37, 39, 42 and 47 marked in the upper part.

Outside the wave, the electric field on the decreasing ramp solves Eq. (4) with negligible space and time derivatives. Then $v(E)=J/r$, which implies $E(r,t)=E_1(J/r)$ outside the wave. If $J \ll r$, the first branch of $v(E)$ is linear, and we have $E(r,t) \approx J/r$. The area under this stationary field profile is $\phi_{out} = \int_{r_c}^{r_a} E_1(J/r) dr \approx J \ln(r_a/r_c)$. The equation for J is now

obtained by time differencing the bias condition, $\phi = \phi_{in} + \phi_{out}$, with the result

$$\frac{dJ}{dt} = \frac{1}{\ln(r_a/r_c)} \left(\frac{\pi}{4} - \frac{J E_+}{r_w} \right). \quad (9)$$

When the wave is far from the cathode, the second term in the right hand side of this equation is small compared with the first one. Then J is approximately linear, with slope $\pi/[4 \ln(r_a/r_c)]$. This behavior can be observed in Fig. 5. After the dipole vanishes, a new wave is nucleated at the cathode, and this process explains the shape of the current trace during the rest of one oscillation period. The description of this latter process is more technical and it will be published elsewhere.

More complicated patterns can be obtained by playing with the number and location of point contacts. Figure 7 shows a sample with two cathodes and two anodes located at the vertices of a square. Axisymmetric waves are nucleated at the cathodes, collide, form a eight shaped wave, which later disappears. The resulting self-oscillation of the current is also shown in Fig. 7.

In conclusion, we have presented a number of spatiotemporal patterns associated to Gunn self-oscillations of the current in rectangular samples with point contacts. Several features of these oscillations can be interpreted in the light of the known theory for 1D samples and its extension to axisymmetric geometries sketched here. Finding a general theory of these patterns is clearly a worthwhile future investigation.

We thank F. J. Higuera, B. García-Archilla, and I. R. Cantalapiedra for helpful discussions. R. E. acknowledges support of the Fundación Carlos III. This work has been supported by the Spanish DGES Grant No. PB98-0142-C04-01.

-
- [1] V. L. Bonch-Bruевич, I. P. Zvyagin, and A. G. Mironov, *Domain Electrical Instabilities in Semiconductors* (Consultants Bureau, New York, 1975).
- [2] M. P. Shaw, H. L. Grubin, and P. R. Solomon, *The Gunn-Hilsum Effect* (Academic Press, New York, 1979).
- [3] E. Schöll, *Nonequilibrium Phase Transitions in Semiconductors* (Springer, Berlin, 1987).
- [4] *Nonlinear Dynamics and Pattern Formation in Semiconductors and Devices*, edited by, F.-J. Niedernostheide, Springer Proceedings in Physics Vol. 79 (Springer-Verlag, Berlin, 1995).
- [5] J.B. Gunn, *Solid State Commun.* **1**, 1 (1963).
- [6] H. Kroemer, *IEEE Trans. Electron Devices* **13**, 27 (1966).
- [7] A.M. Kahn, D.J. Mar, and R.M. Westervelt, *Phys. Rev. B* **45**, 8342 (1992); *Phys. Rev. Lett.* **68**, 369 (1992); M.J. Bergmann *et al.*, *Phys. Rev. B* **53**, 1327 (1996).
- [8] B. Willing and J.C. Maan, *Phys. Rev. B* **49**, 13 995 (1994); B. Willing, Ph.D. thesis, University of Nijmegen, 1994.
- [9] F. Piazza *et al.*, *Appl. Phys. Lett.* **69**, 1909 (1996).
- [10] M. Büttiker and H. Thomas, *Phys. Rev. Lett.* **38**, 78 (1977).
- [11] L.L. Bonilla *et al.*, *Phys. Rev. B* **50**, 8644 (1994); J. Kastrup *et al.*, *ibid.* **55**, 2476 (1997); L.L. Bonilla *et al.*, *SIAM (Soc. Ind. Appl. Math.) J. Appl. Math.* **57**, 1588 (1997).
- [12] K. Aoki and K. Yamamoto, *Phys. Lett. A* **98**, 72 (1983).
- [13] J. Peinke *et al.*, *Phys. Lett. A* **108**, 407 (1985).
- [14] E.G. Gwinn and R.M. Westervelt, *Phys. Rev. Lett.* **57**, 1060 (1986); **59**, 247 (1987).
- [15] F.J. Higuera and L.L. Bonilla, *Physica D* **57**, 161 (1992).
- [16] L.L. Bonilla and I.R. Cantalapiedra, *Phys. Rev. E* **56**, 3628 (1997); L.L. Bonilla *et al.*, *Physica D* **108**, 168 (1997); L.L. Bonilla *et al.*, *Phys. Rev. E* **56**, 1500 (1997).
- [17] W. Eberle *et al.*, *Appl. Phys. Lett.* **68**, 3329 (1996).
- [18] L. L. Bonilla, R. Escobedo, and F. J. Higuera (unpublished).